Araştırma Makalesi / Research Article

Synthesis and Spectroscopic Characterization of Novel Pyridine-based N-acyl Hydrazone Derivatives and Molecular Docking Studies on Glucosamine-6-Phosphate

Derya VURAL[1]* 🆔, Selbi KESKİN[2] 🆔

Abstract

Antimicrobial resistance in infectious diseases caused by organisms such as bacteria, fungi, viruses, and parasites has led to an increase in studies and demands for new antimicrobial drug development. The compounds including pyridine and N-acylhydrazone skeletons in their structures have a large application area in drug discovery due to their anticancer, anti-tubercular, anti-bacterial and anti-fungal activities. Here, the novel N-acyl-hydrazone derivatives, (*E*)-2-oxo-N'-(2,3,4-trimethoxybenzylidene)-1,2-dihydropyridine-3-carbohydrazide and (*E*)-N'-(1-(4-bromophenyl) ethylidene)-2-oxo-1,2-dihydropyridine-3-carbohydrazide were synthesized through a multistep reaction sequence. The structures of newly synthesized compounds were established on the basis of IR, 1D and 2D NMR spectra and mass spectral data. The theoretical electronic structure analysis was performed by density functional theory (DFT) at the B3LYP level with the 6-311++G(d,p) basis set in the gas phase of synthesized compounds. The newly synthesized compounds were docked on glucosamine-6 phosphate synthase to determine potential interactions between the analyzed compounds and its active site due to its role in microbial cell wall synthesis. The possibilities of these compounds to being active for antimycobacterial and antituberculosis have been found as quite high, and their interactions in the binding site have been determined with the range of binding affinity, [-7.1, -7.3] kcal/mol, respectively.

Keywords: N-acylhydrazone, nitrogen containing heterocycles, molecular docking, glucosamine-6 phosphate.

Yeni Piridin Bazlı N-Açil Hidrazon Türevlerinin Sentezi ve Spektroskopik Karakterizasyonu ve Glukozamin-6-Fosfat Üzerine Moleküler Yerleştirme Çalışmaları

Öz

Bakteri, mantar, virüs ve parazit gibi organizmaların neden olduğu bulaşıcı hastalıklardaki antimikrobiyal direnç yeni antimikrobiyal ilaç geliştirmeye yönelik çalışmaların ve taleplerin artmasına neden olmuştur. Temel yapısında piridin ve N-açilhidrazon içeren bileşikler, antikanser, tüberküloz, anti-bakteriyel ve anti-fungal aktivitelerinden dolayı ilaç tasarımında geniş bir uygulama alanına sahiptir. Bu çalışmada, yeni N-açil-hidrazon türevleri, (*E*)-2-okso-N'-(2,3,4-trimetoksibenziliden)-1,2-dihidropiridin-3-karbohidrazid   ve   (*E*)-N'-(1-(4-bromofenil)etiliden)-2-okso-1,2-dihidropiridin-3-karbohidrazid, çok aşamalı bir reaksiyon dizisi yoluyla sentezlenmiştir. Yeni sentezlenen bileşiklerin yapıları IR, 1D ve 2D NMR spektrumları ve kütle spektral verileri kullanılarak belirlenmiştir. Teorik elektronik yapı analizleri ise 6-311++G(d,p) baz setine sahip B3LYP seviyesinde yoğunluk fonksiyonel teorisi kullanılarak gaz fazında gerçekleştirilmiştir. Glukozamin-6 fosfat sentaz proteininin mikrobiyal hücre duvarı sentezindeki rolü nedeniyle, yeni sentezlenen bileşiklerin bu moleküller aralarında gerçekleşebilecek etkileşimlerini belirlemek için moleküler yerleştirme analizi yapılmıştır. Bu bileşiklerin antimikobakteriyel ve antitüberküloz aktivitelerinin oldukça yüksek olduğu belirlenerek bağlanma bölgesindeki etkileşimleri de sırasıyla [-7.1, -7.3] kcal/mol bağlanma afinitesi olarak belirlenmiştir.

Anahtar Kelimeler: N-açil hidrazon, azot içeren heterohalkalı bileşikler, moleküler yerleştirme, glukozamin-6 fosfat.

[1]Giresun University, Department of Physics, Faculty of Arts and Sciences, Giresun, Turkey,   derya.vural@giresun.edu.tr
[2]Giresun University, Department of Chemistry, Faculty of Arts and Sciences, Giresun, Turkey,   selbi.keskin@giresun.edu.tr

[1]https://orcid.org/0000-0002-0120-3024   [2]https://orcid.org/0000-0003-0664-9903

1. Introduction

Microbial infections are the growing threat to human health due to the antimicrobial resistance. Since organism, bacteria, fungi, viruses, and parasites, causing to infectious diseases varies over time, the resistance to antimicrobial medicines increases and they become ineffective. It has been reported that the resistance of the against antibiotics increases for bacterial infections. The rising in the drug-resistant Mycobacterium tuberculosis cases estimated by the World Health Organization (WHO) also reveals the risk of the spreading globally (*World Health Organization WHO*, 2021).

The decrease in the effect of antibiotics has led to a new potential drugs search. In drug discovery, molecular docking is one of the commonly used techniques to test the suitability of chemical compounds and to decrease a chemical search list (M. T. Ali et al., 2018; Almutairi et al., 2018; Banerjee et al., 2011; El Sayed et al., 2018; More et al., 2014; Shyma et al., 2013; Wang et al., 2017). Glucosamine-6-Phosphate synthase, an enzyme present in microbial cells, plays an important role in the production of Glucosamine-6-Phosphate (Chmara et al., 1986; Fikrika et al., 2016). Compounds including N-benzyl-2,2,2 trifluoroacetamide (Fikrika et al., 2016), N-heterocyclic (Askri et al., 2022), novel 2,5-disubstituted-1,3,4-oxadiazole derivatives (Tok et al., 2021) have been investigated as a potential inhibitor of Glucosamine-6-Phosphate synthase to suppress the production of glucosamine-6-phosphate.

Quantitative structure activity relationship (QSAR) analyses aim to provide information about relationships between structural properties of chemical compounds and biological activities of compounds, for instance a QSAR may be developed to explore how a pyridine skeleton and other moieties (including N-acylhydrazone) demonstrate a broad spectrum of biological activities such as antimicrobial and antimycobacterial activities (Narang et al., 2011, 2012). In a wide perspective, pyridine derivatives play a vital role in medicinal chemistry and it has been reported that there are many drugs consisting of pyridine moiety with a broad spectrum of pharmacological and therapeutic properties including anticancer (Shah et al., 2018), antimicrobial (Muluk et al., 2019), antioxidant (Kotb et al., 2017), and anti-inflammatory (Kandasamy et al., 2019). Similarly, the hydrazone functional group is considered an important functionality in pharmacology since it provides strategic pharmacophore because its unique structure is capable of acting as hydrogen bond acceptors and/or donors to interact with various amino acids of the biological targets. N-acylhydrazones, hydrazide-hydrazone derivatives, are crucial for pharmacology and play an important role for the antimicrobial activity that is why it is important for synthetic organic chemistry. They possess lots of biological activities such as antibacterial (Pomarnacka et al., 2006), antituberculosis (Bedia et al., 2006) and anticonvulsant (Ragavendran et al., 2007). It is stated in some papers and patents in the literature that pyridine-based hydrazones possess important pharmacological properties such as antimicrobial

(Neuman, 2018; Soujanya et al., 2017; Ukrainets et al., 2007), antifungal (Backes et al., 2015), antibacterial (Ali et al., 2020; Morjan et al., 2014) and anti-inflammatory (Khalil et al., 2013).

In this study, we discuss the synthesis procedure of (*E*)-2-oxo-N'-(2,3,4-trimethoxybenzylidene)-1,2-dihydropyridine-3-carbohydrazide (Ligand **1**) and (*E*)-N'-(1-(4-bromophenyl) ethylidene)-2-oxo-1,2-dihydropyridine-3-carbohydrazide (Ligand **2**), the experimental and computational spectroscopic characterization completed by using NMR, FT-IR spectroscopic techniques and Gaussian 09W. (Scheme 1) The goal is to determine the role of the dihydropyridine-carbohydrazide derivatives in the inactivation of Glucosamine-6-Phosphate synthase, which could be important to find better antimicrobials. Here, we performed the molecular docking of the newly synthesized compounds on glucosamine-6-phosphate synthase to determine the inter-molecular interactions and predict their behavior in the binding sites.


Ligand 1   Ligand 2
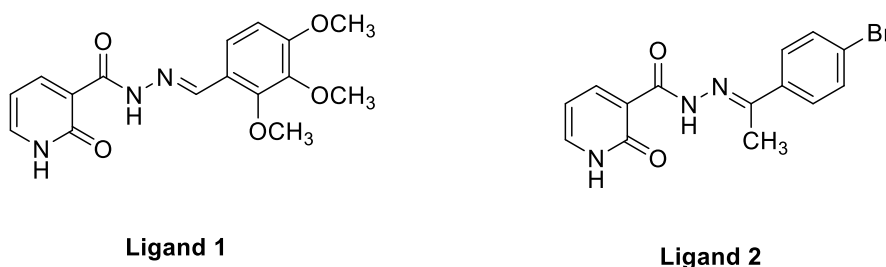
Scheme 1

2. Materials and Methods

2.1. Chemistry

The reaction scheme employed for the synthesis of target molecules are given in Scheme 2. One of the key compounds of the condensation reaction is hydrazide **3** and it was synthesized starting from the commercially available 2-hydroxy-nicotinic acid (**1**) in two steps. Firstly, 2-hydroxy-nicotinic acid (**1**) was refluxed in ethanol in the presence of catalytic amount of H_2SO_4 (He et al., 2012). The product, the compound **2**, was then reacted with hydrazine monohydrate in methanol at reflux temperature to get the key compound **3** similar to literature procedure (David et al., 2010). The condensation reaction between the compound **3** and trimethoxy-substituted aldehyde **4** in ethanol resulted in the formation of N-acyl hydrazone derivative (Ligand **1**). Ligand **2** was also synthesized from the condensation reaction between the hydrazide **3** and 4-bromoacetophenone (**5**). (Scheme 2) The structures of newly synthesized N-acylhydrazones were characterized by FT-IR, NMR, and mass spectroscopy techniques.

Scheme 2
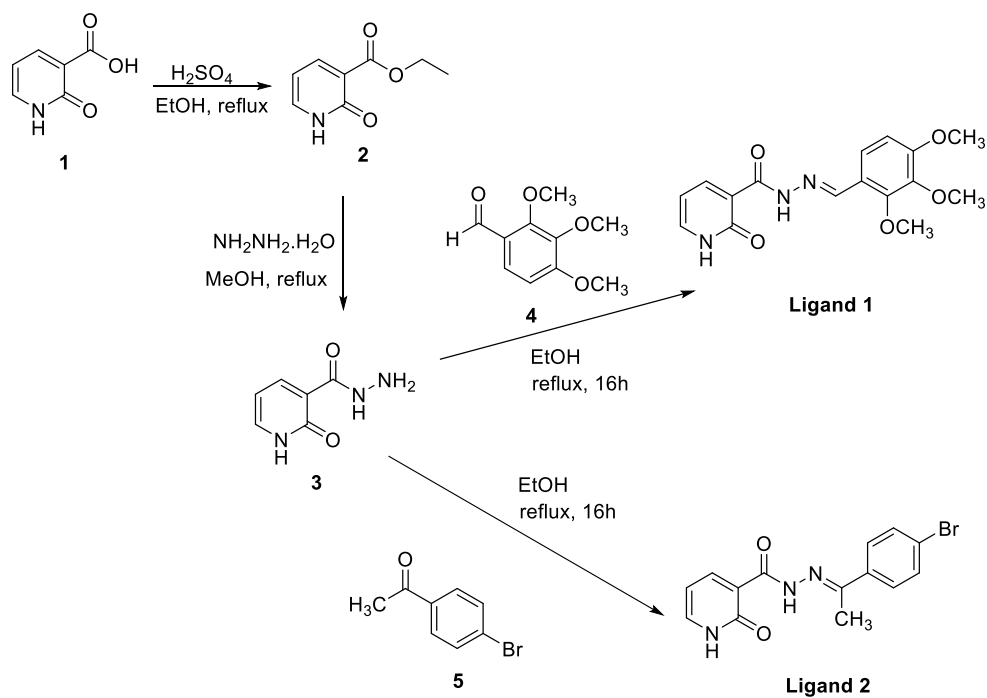
2.2.Experimental

All materials were purchased from commercial sources and they were used without further purification unless otherwise specified. Reactions were monitored by thin-layer chromatography (TLC) with fluorescent indicator visualizable at 254 nm and 365 nm. Melting points were determined by using a Barnstead electrothermal 9200 series digital apparatus using open glass capillaries. Fourier Transform Infrared (FT-IR) (400-4000 cm^{-1}) spectra were recorded using Thermo Scientific Nicolet IS10 ATR FT-IR spectrometer. Band positions were reported in reciprocal centimeters (cm^{-1}). ^{1}H NMR (400 MHz) spectra and ^{13}C NMR (100 MHz) spectra, APT, HSQC and HMBC NMR Spectra of the compounds were recorded on a Bruker Ascend 400 (100)-MHz spectrometer with DMSO-*d6* or CDCl$_3$ as the solvent. Chemical shifts were reported (λ) relative to Me$_4$Si as internal standard and coupling constants, *J*, were reported in hertz (Hz). Mass spectrums of the compounds were performed using Agilent 1260 Infinity Series LC-MS/Q-TOF at the Giresun University Central Research and Application Laboratory.

The synthesis of Ethyl 2-oxo-1,2-dihydropyridine-3-carboxylate (2) (He et al., 2012)

To a stirred solution of 2-hydroxy nicotinic acid (**1**) (1.0 g, 7.20 mmol) in ethanol (20 mL), concentrated sulfuric acid (7.20 mL) was added. The formed solution was refluxed overnight. The

reaction mixture was monitored by TLC. After the reaction was complete, ethanol was evaporated under reduced pressure. The residue was treated with a solution of $NaHCO_3$ (pH = 7-8) and then extracted with dichloromethane. The organic layers were washed with brine and dried over anhydrous Na_2SO_4. Solvent was evaporated until dryness to get the title compound (**2**) as a white solid. (0.9 g, 80%). ^{1}H NMR (400 MHz, CDCl₃) 13.61 (s, 1H), 8.26 (br d, $J = 7.1$ Hz, 1H), 7.78 (br d, $J = 5.6$ Hz, 1H), 6.40 (t, $J = 6.3$ Hz, 1H), 4.36 (q, $J = 6.9$ Hz, 2H), 1.37 (t, $J = 6.9$ Hz, 3H).

The synthesis of 2-oxo-1,2-dihydropyridine-3-carbohydrazide (3)

Ethyl 2-oxo-1,2-dihydropyridine-3-carboxylate (**2**) (0.2 g, 1.2 mmol) was refluxed with hydrazine monohydrate (0.5 mL) in methanol for 18h. After cooling of the reaction mixture, the formed precipited was filtered off and wash with ethanol and white solid compound was dried. (172 mg, 94%). ^{1}H-NMR (DMSO-d_6, 400 MHz): δ 12.45 (br s, 1H), 10.56 (s, 1H), 8.30 (dd, $J = 7.2, 2.2$ Hz, 1H), 7.67 (dd, $J = 6.3, 2.2$ Hz, 1H), 6.51 (dd, $J = 7.1, 6.3$ Hz, 1H), 4.64 (br s, 2H). ^{13}C-NMR (DMSO-d_6, 100 MHz): δ 163.0, 162.2, 144.0, 139.4, 120.0, 106.9.

General procedure for the synthesis of N-acylhydrazone derivatives

A mixture of hydrazide **3** (1 mmol) and the substituted benzaldehyde or acetophenone (1 mmol) in EtOH (10 mL) was refluxed overnight (Demurtas et al., 2019). After cooling the reaction mixture, precipitate was formed and it was filtered off and washed with ethanol. The product of the reaction was purified by crystallization from ethanol.

(E)-2-oxo-N'-(2,3,4-trimethoxybenzylidene)-1,2-dihydropyridine-3-*carbohydrazide* (Ligand 1)

Yield: 94%, m.p: 208-209 °C. ^{1}H NMR (DMSO- d_6, 400 MHz) δ 12.90 (s, 1H, O=C-NH-N), 12.71 (br s, 1H, NH), 8.42 (dd, $J = 7.0, 1.3$ Hz, 1H), 8.37 (br s, 1H, C=NH), 7.78 (d, $J = 5.0$ Hz, 1H), 7.62 (d, $J = 8.8$ Hz, 1H, aromatic H), 6.93 (d, $J = 9.0$ Hz, 1H, aromatic H), 6.57 (t, $J = 6.7$ Hz, 1H), 3.85 (s, 3H, OCH₃), 3.84 (s, 3H, OCH₃), 3.76 (s, 3H, OCH₃). ^{13}C NMR (DMSO-d_6, 100 MHz) δ 162.5, 160.4, 155.8, 153.1, 145.3, 144.0, 141.9, 140.5, 121.4, 120.5, 120.1, 109.1, 107.4, 62.3, 60.9, 56.4. IR (KBr, cm^{-1}) 3141 (N-H), 3010 (N-H), 2929, 2825(arom C-H), 1684 (C=O), 1610 (C=O), 1536, 1494, 1285 (arom. C=C, C=N, C-N, Ar-O-C), 1086, 1004, 777. HRMS-TOF [M+H]$^+$ Calculated for $C_{16}H_{18}N_3O_5$ 332.1241, found: 332.1720.

(E)-N'-(1-(4-bromophenyl)   ethylidene)-2-oxo-1,2-dihydropyridine-3-*carbohydrazide* **(Ligand 2)**

Yield: 92%, m.p: 301-302 °C. ^{1}H NMR (DMSO-d_6, 400 MHz) δ 13.16 (s, 1H, O=C-NH-N), 8.46 (d, J = 7.4 Hz, 1H), 7.95 – 7.74 (m, 4H), 7.63 (d, J = 8.0 Hz, 2H), 6.59 (t, J = 6.8 Hz, 1H), 2.30 (s, 3H). ^{13}C NMR (DMSO-d_6, 100 MHz) δ 162.7, 160.2, 150.8, 145.1, 140.4, 137.2, 131.5 (2C), 128.6 (2C), 123.0, 119.8, 107.3, 13.9. IR (KBr, cm^{-1}) 3104 (N-H), 3072 (N-H), 2953 (arom C-H), 1657 (C=O), 1529, 1484, 1313, 1213 (arom. C=C, C=N, C-N), 764, 534 (C-Br). HRMS-TOF [M+H]$^+$ Calculated for $C_{14}H_{13}BrN_3O_2$ 334.0186, found: 334.0215.

2.3. Computational Procedures

2.3.1. Optimization and NMR calculation

Geometry optimization of ligands ((*E*)-2-oxo-N'-(2,3,4-trimethoxybenzylidene)-1,2-dihydropyridine-3-carbohydrazide and (*E*)-N'-(1-(4-bromophenyl) ethylidene)-2-oxo-1,2-dihydropyridine-3-carbohydrazide) was performed using Density Functional Theory (DFT) method with the B3LYP functional form and 6-311++(d,p) basis set (Becke, 1993; Lee et al., 1988). The calculations of ligands were performed using Gaussian 09W (Frisch et al., 2009) at 298.15 Kelvin and 1 atm. For the newly synthesized ligand **1** and ligand **2**, the calculated optimized structure parameters such as bond lengths, bond angles and dihedral angles were determined and the visual molecular optimized structures were illustrated by using the GaussView5.0 (Dennington et al., 2009). The thermochemical properties were also obtained in the optimization process. For ^{1}H and ^{13}C NMR calculation, the geometrical optimization was repeated in DMSO solvent at IEF-PCM solvation model (Cancès et al., 1997), and then GIAO method was used (Ditchfield, 1974; Wolinski et al., 1990).

2.3.2. Molecular Docking

Molecular docking analysis was performed using the popular docking program AutoDock Vina (Trott et al., 2010). The three dimensional structure form of glucosamine-6-phosphate synthase (PDB ID:2VF5) was obtained from a protein data bank (see Figure 3) (Mouilleron et al., 2008). Receptor data were opened using AutoDockTools (ADT) 1.5.6 (Morris et al., 2009) to remove the natural ligand that was still attached to it before the water molecules were removed, followed by adding the nonpolar hydrogen atoms. The protein file then was saved in AutoDock pdbqt format and ready to be used for docking. Similarly, both of the ligands were prepared using AutoDockTools and the searched box size was chosen as 50Åx50Åx50Å with the grid spacing of 0.375 Å at center position (29.32,
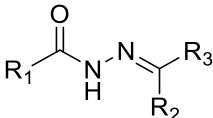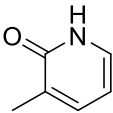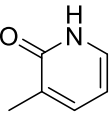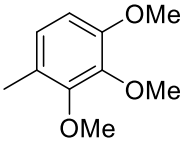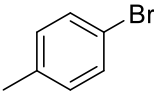
18.375, -3.793). The exhaustiveness was chosen as 8. The interactions between ligand molecules and glucosamine-6-phosphate synthase were analyzed using Discovery Studio Visualizer (*BIOVIA, Dassault Systemes, Discovery Studio Modeling Environment, Release 2017, San Diego*, 2016).

3. Findings and Discussion

3.1. Molecular Structure and Thermochemical Properties

The structure of ligands is generalized as (R_1-CO-NH-N=C-R_2-R_3) and the substituents R_1, R_2 and R_3 are listed in Table 1.

Table 1. The list of the sub-groups in the structure of ligands

	Ligand 1	Ligand 2
R_1		
R_2	-H	-CH_3
R_3		

The optimized structure parameters and atom coordinates of ligand **1** and ligand **2** molecules are in Supporting Information (S.I.) file (see Table S1-S4), and their visual presentations, the atom numbering scheme are shown in Figure 1. The thermochemical properties of the optimized geometrical structure of both ligand molecules given in Table 2 indicate that the larger contribution to thermal energy, entropy, and enthalpy arise from the vibrational part since the electronic contribution is 0.000, and the total values is found as 214.792 and 161.822 kcal/mol for ligand **1** and ligand **2**, respectively. It has been also found that the total electronic energy value, E(RB3LYP) = -3429.7996, for ligand **2** is found as larger than that, E(RB3LYP) = -1160.5837, for ligand **1**.
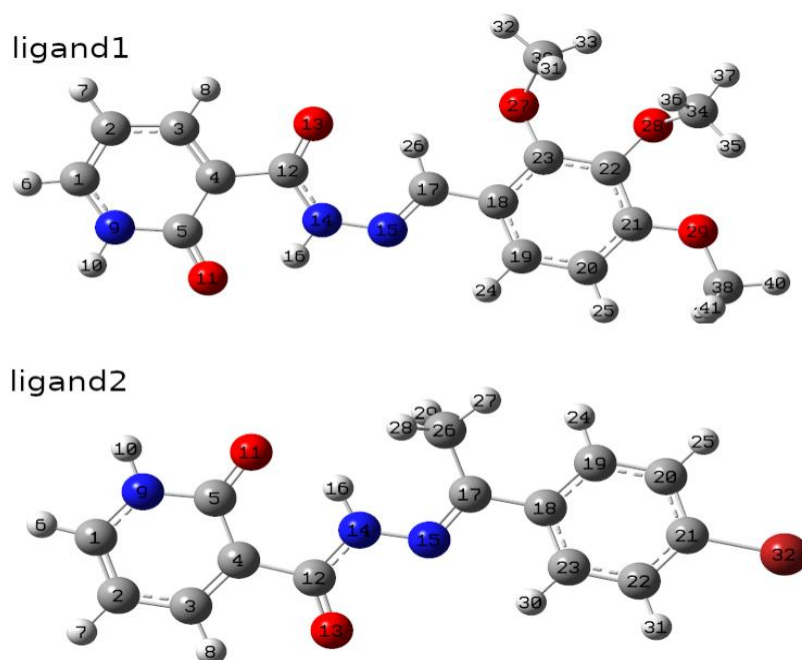
Figure 1. The optimized molecular structure of (*E*)-2-oxo-N'-(2,3,4-trimethoxybenzylidene)-1,2-dihydropyridine-3-carbohydrazide (Ligand **1**) and (*E*)-N'-(1-(4-bromophenyl) ethylidene)-2-oxo-1,2-dihydropyridine-3-carbohydrazide (Ligand **2**) obtained using GaussView5.0.

To understand the optimized geometrical structure, having the minimum potential energy surface, the orientation of two intersecting planes defined with C12, N14, N15, C17 atoms and of R_1 and R_3 rings around these planes has been investigated. The dihedral angle of C12-N14-N15-C17 is found as -5.96° and -177.67° for ligand **1** and ligand **2**, respectively. These results indicate that ligand molecules are not planar, which is consistent with molecules having sp^2 and sp^3 hybridized atoms. The C3-C4-C12-N14 and N15-C17-C18-C19 torsional angles, indicating the distortion of the R_1 and R_3 rings from the plane surface between them, are found as -178.43° and -2.63° for ligand **1**, and -179.38° and 164.61° for ligand **2**. While the C-C-C angles of R_1 and R_3 rings vary between 118° and 123°, slightly distorted from the typical hexagonal angle of 120°, the angles of C1-N9-C5, C2-C1-N9 and C4-C5-N9 are found as 125°, 119° and 114°, respectively.

In R_1 ring, the bond lengths vary between 1.36 Å and 1.42 Å, slightly different from the bond length 1.33 Å of a pyridine ring, except the slightly higher C4-C5 bond length, 1.46 Å, due to the O-atom bonded to C5. The bond length between C12 and C4 (R1 group) is found as 1.51 Å for both of ligand molecules, since it between C17 and C18 (R$_3$ group) is slightly longer for ligand **2** than ligand **1** (1.47 Å (ligand **1**) < 1.49 Å (ligand **2**)) due to the CH$_3$ substitution to C17 of ligand **2**. The length of C-C bond in benzene ring of ligand **1** and ligand **2** varies from 1.39 Å to 1.4 Å. The C=O bond lengths in both ligand molecules are found approximately as 1.22 Å while C-O bonds in R$_3$ ring of ligand **1** molecule varies between 1.36 Å and 1.42 Å. The bonds only existing in ligand **2** molecule are C21-Br32 with the lengths of 1.92 Å. The C-H and N-H bonds are approximately found as 1.09

Å and 1.01 Å, respectively. These values have good agreement with the values in literature (Cai et al., 2011; Fun et al., 2011; Wu et al., 2009).

Table 2. Thermo-chemical properties of ligand **1** and ligand **2** molecules

		Ligand1	Ligand2
Rotational temperatures (Kelvin)		0.03176	0.05493
		0.00401	0.00348
		0.00358	0.00328
Rotational constants (GHZ):		0.66178	1.14450
		0.08347	0.07254
		0.07456	0.06834
Zero-point vibrational energy (Joules/Mol)		837873.8	629991.7
Zero-point correction (Hartree/Particle)		0.31913	0.23995
Thermal correction to Energy		0.34229	0.25788
Thermal correction to Enthalpy		0.34324	0.25882
Thermal correction to Gibbs Free Energy		0.26382	0.19035
Sum of electronic and zero-point Energies		-1160.26458	-3429.55961
Sum of electronic and thermal Energies		-1160.24141	-3429.54168
Sum of electronic and thermal Enthalpies		-1160.24047	-3429.54074
Sum of electronic and thermal Free Energies		-1160.31988	-3429.60921
E (Thermal) **(KCal/Mol)**	Total	214.792	161.822
	Electronic	0.000	0.000
	Translational	0.889	0.889
	Rotational	0.889	0.889
	Vibrational	213.015	160.045
CV **Cal/Mol-Kelvin**	Total	84.989	67.060
	Electronic	0.000	0.000
	Translational	2.981	2.981
	Rotational	2.981	2.981
	Vibrational	79.027	61.098
S **Cal/Mol-Kelvin**	Total	167.145	144.106
	Electronic	0.000	0.000
	Translational	43.287	43.304
	Rotational	35.611	35.292
	Vibrational	88.248	65.510
E(RB3LYP)		-1160.58371	-3429.79956

3.2. Spectroscopic characterization

Target compounds were experimentally characterized by the spectroscopic techniques (Nuclear Magnetic Resonance Spectroscopy (NMR), High-Resolution Mass Spectrometry (HRMS) and Fourier Transform Infrared Spectroscopy (FTIR)). Assignments of all protons and carbons in the target structures were made by the help of 1D and 2D NMR spectra. The ^{1}H-NMR, ^{13}C-NMR and 2D NMR spectra (APT, COSY, HSQC and HMBC) measured in DMSO-*d6* of all the compounds were given in Figures S1-S14 (see SI). The IR spectra of ligands showed the absorption bands of the NH groups in the structures at around 3100 cm^{-1}. In addition, in the region of v = 1683–1620 cm^{-1}, the absorption bands of C = O groups in the structure of the ligands were observed (see SI, Figure S15-

S16). The optimized structural geometries in DMSO with IEF-PCM model of the ligand **1** and **2** were used to compute NMR chemical shifts using same solvation selection at the B3LYP/6-311G++(d,p) level with GIAO method. Table 3 shows the computed and experimental ^{1}H and ^{13}C NMR chemical shifts of the ligand **2.**

Table 3: The experimental and calculated ^{1}H-NMR and ^{13}C-NMR chemical shifts of the ligand **2** (all values are in ppm)

Atoms	$\delta_{exp.}$	$\delta_{calc.}$	Atoms	$\delta_{exp.}$	$\delta_{calc.}$
H6	7.82	7.78	C1	140.4	145.7
H7	6.59	6.67	C2	107.3	112.1
H8	8.46	8.87	C3	145.1	151.3
H10	7.84	8.75	C4	119.8	125.3
H16	13.16	12.37	C5	162.7	166.7
H24	7.80	8.27	C12	160.2	165.4
H30	7.80	7.83	C17	150.8	157.5
H25	7.63	7.78	C18	137.2	145.4
H31	7.63	7.60	C19	128.6	133.8
H27	2.30	2.64	C23	128.6	133.0
H28	2.30	2.23	C20	131.5	136.8
H29	2.30	2.23	C22	131.5	136.8
			C21	123.0	147.24
			C27	13.9	13.9

When examined the ^{1}H-NMR spectrum of the ligand **2**, it was seen that there are three hydrogens resonating separately and two hydrogens having same environment, resonating together. Moreover, since four hydrogens resonate in very close regions to each other, their signals were seen to coincide with each other and seem as multiplet between 7.95-7.74 ppm. However, all the carbons and hydrogens were assigned by using 2D NMR spectra and all the spectra were seen in Figures S4-S9 (see SI). H6 proton gave resonance signal at around 7.82 ppm as multiplet due to the overlapping of another peak in the experimental spectrum while it was computed at 7.78 ppm. The H7 was split by H6 and H8, and it resonated at 6.59 ppm as a triplet with the 6.8 Hz coupling constant value experimentally and its theoretically calculated resonance signal value is 6.67 ppm. The H8 was recorded as a doublet at 8.46 ppm with the value of coupling constant 6.53 Hz splitting by H7 proton experimentally and it is calculated at 8.87 ppm. The resonance signal of NH proton on the ring, H10, was observed at 7.84 ppm as a broad singlet. The calculated value for H10 is 8.75 ppm. The amide NH proton, H16, was theoretically calculated as 12.37 ppm while recorded experimentally at 13.16 ppm as a singlet. About the benzene protons, it is clearly seen that these protons resonate as AA'BB' system. The A part of the AA'BB' system, the H24 and H30, was observed in the experimental spectrum at around 7.80 ppm as multiplet due to the overlapping with different signals while B part of the AA'BB' system, H25 and H31, was appeared as a doublet at 7.63 ppm with the value of 7.35 Hz of coupling constant. The aromatic protons H24 and H30 were computed at 7.83 and 8.27 ppm

while the H25 and H31 were theoretically detected at 7.78 and 7.60 ppm, respectively. The methyl protons (H27, H28 and H29) were observed as singlet at 2.30 ppm in the experimental ^{1}H-NMR spectrum and theoretically obtained at 2.64 ppm and 2.23 ppm. Overall, comparison of the ^{1}H-NMR chemical shifts for ligand **2** indicate a good agreement between experiment and theory agree.

The assignment of carbons was done by the help of HSQC and HMBC spectrum. The carbons bonded to hydrogen were easily determined by HSQC spectrum. The H6 correlates with the carbon signal at 140.4 ppm, and it is the C1 carbon calculated theoretically at 145.7 ppm. It was determined that resonance signal of the C2 carbon connected to the H7 proton was at 107.3 ppm in the experimental ^{13}C-NMR spectrum while calculating at 112.1 ppm theoretically. The C3 carbon was computed at 151.3 ppm and detected experimentally at 145.1 ppm. For the assignment of carbonyl carbon atoms, the HMBC spectrum was used. The correlations between H8 (at 8.46 ppm) and the carbons resonating at 140.4, 162.7 and 160.2 ppm were determined. It means that the signals at the 162.7 and 160.2 ppm belong to the carbonyl carbons in the structure of the ligand **2** because the signal at 140.4 ppm belongs to the C1. Additionally, it was seen that the carbon signal at 162.7 ppm correlated both H8 and H6 and it is the proof that this signal (at 162.7) belongs to C5 carbon which was calculated theoretically at 166.7 ppm. The C12 carbon signal was observed at 160.2 ppm (exp.) and 165.4 ppm (calc.) in the ^{13}C-NMR spectrum. The peak at 150.8 correlates with H16, H30 and CH$_3$ protons in the HMBC spectrum over three bonds and it is concluded that this signal belongs to the imine carbon atom, the C17 carbon calculating at 157.5 ppm as theoretically. The computed resonance signal of the C18 carbon was at 145.4 ppm and it was experimentally found at 137.2 ppm. The C18 signal correlates with H31 and CH$_3$ protons. The C19 and C23 carbons gave resonance signal at 128.6 ppm together as expected although they gave resonation separately at 133.8 and 133.0 ppm according to calculated results. Also, the C20 and C22 carbons were appeared at 131.5 ppm together in the experimental ^{13}C-NMR spectrum and calculated at 136.8 ppm. The C21 carbon at 123.0 ppm determined from the correlations with H30 proton over 3-bonds and H31 proton over 2 bonds in the HMBC spectrum was calculated at 147.25 ppm as theoretically. This difference can be explained by heavy atom effect. In the first sight, it is expected that bromine withdraw the electron from the aromatic ring and the chemical shift value of C21 carbon should be shifted to downfield due to the electronegativity of bromine atom. However, the experimental value shows that this ipso carbon, C21, shifted to high-field region (123.0 ppm) and chemical shift follows an opposite trend than expected. Br has a wide electron cloud distribution. This electron cloud has very important effect on shielding of C21 and it immerses the carbon within an electron cloud. It is the reason of diamagnetic shielding around the C21 carbon nucleus anda high-field shift.

Figure 2. NOESY spectrum of the ligand **2**

After assignment of all hydrogen and carbon atoms, NOESY NMR experiment of the ligand **2** was underwent to identify the stereochemistry (Figure 2). When examined NOESY spectrum of the ligand **2**, NOE signal was observed between the hydrazide NH at 13.16 ppm and methyl protons resonating at 2.30 ppm. It is expected to observe in the E isomer not in the Z-izomer. (Scheme 3)

(*E*)-isomer

(*Z*)-isomer
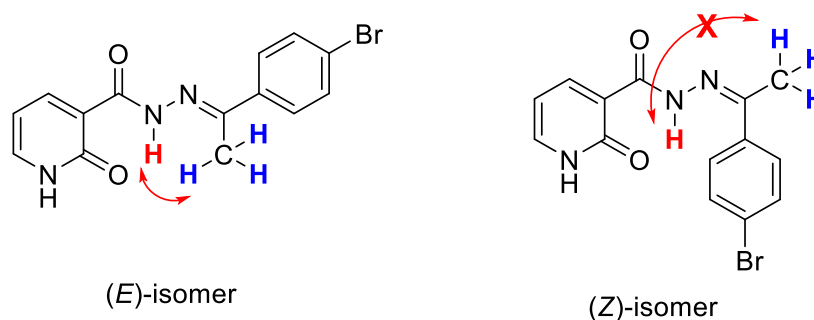
Scheme 3

Table 4 shows the comparison of the experimental and theoretical ^{1}H-NMR and ^{13}C-NMR chemical shifts of the ligand **1** in ppm. All the assignments were done by using 1D and 2D NMR spectra seen in Figures S10-S14 (see SI). In the structure of ligand **1**, there are three methoxy groups connected to the benzene ring. While methoxy protons of H35, H36, H37 were recorded at 3.76 ppm as singlet, the methoxy protons of H31, H32, H33 and H39, H40, H41 were detected at 3.85 ppm and 3.84 ppm, respectively as experimentally. All of the methoxy protons were computed at the interval of 3.33-4.81 ppm theoretically.

Table 4. The experimental and calculated ^{1}H-NMR and ^{13}C-NMR chemical shifts of the ligand **1** (all values are in ppm)

Atoms	$\delta_{exp.}$	$\delta_{calc.}$	Atoms	$\delta_{exp.}$	$\delta_{calc.}$
H6	7.78	7.73	C1	140.5	145.7
H7	6.57	6.59	C2	107.4	112.1
H8	8.42	8.82	C3	145.3	151.3
H10	8.37	8.7	C4	120.1	125.3
H16	12.90	12.29	C5	162.5	166.7
H24	7.62	8.05	C12	160.4	165.4
H26	12.71	10.78	C17	144.0	157.5
H25	6.93	6.79	C18	120.5	145.4
H31	3.85	3.52	C19	121.4	133.8
H32	3.85	4.14	C20	109.1	136.8
H33	3.85	4.25	C21	155.8	147.24
H35	3.76	4.81	C22	141.9	136.8
H36	3.76	3.33	C23	153.1	133.0
H37	3.76	3.93	C30	62.3	62.79
H39	3.84	3.80	C34	60.9	60.8
H40	3.84	4.25	C38	56.4	56.4
H41	3.84	3.80			

3.3. Molecular Docking

The biological activities of ligand **1** and ligand **2** were determined by using PASS Web Online (Filimonov et al., 2014). In the results of PASS analysis, Pa and Pi refer to the probability of being active and inactive, respectively. Since the antimycobacterial activities of ligand **1** and ligand **2** were predicted as [Pa, Pi] = [0.730, 0.004] and [Pa, Pi] = [0.775, 0.004], their antituberculosis activities were found as [Pa, Pi] = [0.712, 0.004] and [Pa, Pi] = [0.780, 0.003], respectively. Molecular docking was performed to predict the interaction between ligand molecules and glucosamine-6-phosphate synthase (PDB ID:2VF5) using AutoDock Vina (Figure 3 and Figure S17). The binding affinity for the best binding mode of ligand **1** and ligand **2** is found as -7.1 and -7.3 kcal/mol respectively. The different binding modes for both ligands could be found in Table S5 in S.I. Discovery Studio Visualizer was used to produce two- and three-dimensional docking representations of both ligand molecules. Molecular docking results reveal the interaction occurred between amino acid residue on the glucosamine-6-phosphate synthase and functional group on the ligand molecules. There are three types of interactions: hydrogen bond, electrostatic and hydrophobic interactions. While hydrogen bond and hydrophobic interactions were observed for both ligand molecules, electrostatic interactions were only observed for ligand **1**.

Hydrogen bond interactions between ligand **1** molecule and target protein are formed as N-H…O and C-H…O. Since the conventional hydrogen bond interaction (N-H…O) is formed (i) between O atom of methoxy group of ligand molecule and NH of residues THR302 and SER303 with 2.57, 2.17, and 2.70 Å of interaction distance, (ii) between =O atom on the ring of ligand molecule

and NH of residues ALA353 and ASP354 with 2.95 and 1.94 Å of interaction distance, respectively. The carbon hydrogen bond interaction (C-H…O) is occurred between O atom of residue SER303 and GLU488 and H atoms of methoxy group of ligand molecule, and between H atoms in residues GLY301 and THR302 and O atom of methoxy group of ligand 1. Here, the interaction distance for the carbon hydrogen bonds varies between 3.35 and 3.51 Å.
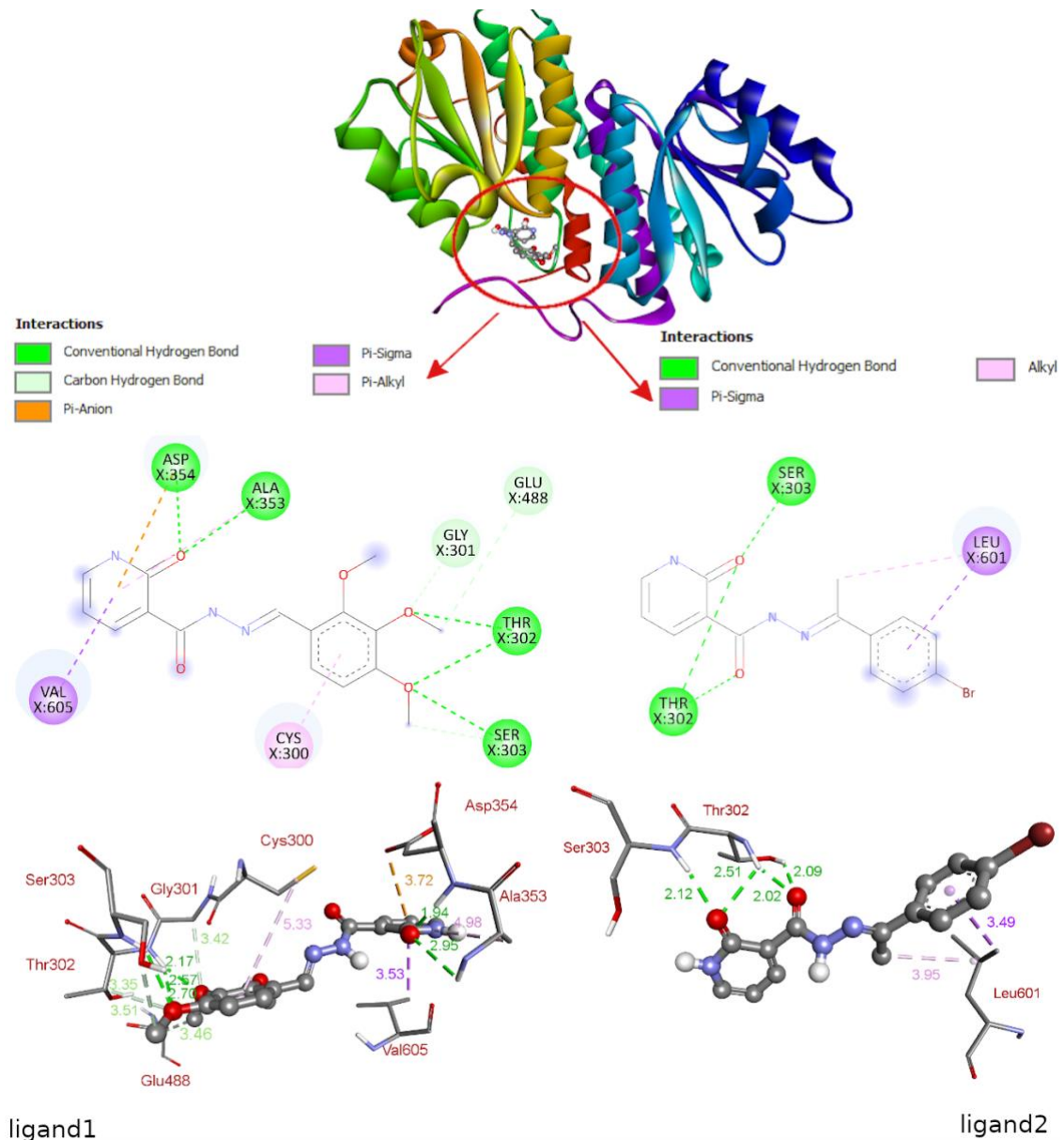

Figure 3. The predicted best binding mode of ligands **1** and **2** to Glucosamine 6-phosphate synthase (PDB ID: 2VF5) with AutoDock Vina predicted binding affinity scores of -7.1 and -7.3 kcal/mol.

The pi-alkyl interactions, one of the hydrophobic interactions, have been observed between the pi-electron cloud over the aromatic groups, dihydropyridinone and benzene rings of ligand molecules, and an alkyl group of residues ALA353 and CYS300 of the glucosamine-6-phosphate

with 4.98 and 5.33 Å of interaction distances, respectively. It has been also observed the pi-sigma interaction between the pyridine ring of ligand and the C atom of residue VAL605 with the 3.53 Å of interaction distance. The pi-anion electrostatic interaction is observed between the electron deficient over the pyridine ring of ligand and the anion on O atom of residue ASP354 and the interaction distance is 3.72 Å.

Hydrogen bond interactions between ligand **2** molecule and target protein are only formed as N-H…O. Here, the conventional hydrogen bond interaction between =O atom of ligand molecule and NH of residues THR302 and SER303 with 2.02, 2.09, 2.12 and 2.51 Å of interaction distance. The hydrophobic interactions were observed between C atom of the residue LEU601 and benzene ring of ligand molecule with 3.49 (pi-sigma), and C atom of methyl group of the ligand and the residue LEU601 with 3.95 of interaction distance (alkyl).

4. Conclusions and Recommendations

The novel N-acylhydrazones, (*E*)-2-oxo-N'-(2,3,4-trimethoxybenzylidene)-1,2-dihydropyridine-3-carbohydrazide (Ligand **1**) and (*E*)-N'-(1-(4-bromophenyl) ethylidene)-2-oxo-1,2-dihydropyridine-3-carbohydrazide (Ligand **2**), were synthesized starting from 2-hydroxynicotinic acid and characterized by spectroscopic techniques both experimentally and computationally. The geometry of the carbohydrazides, ligand **1** and ligand **2**, such as bond lengths, angles, and torsional angles, were characterized using computational technique. Since these two newly synthesized compounds have high activity potential for antimycobacterial and anti-tuberculosis, we were investigated the interaction between the compounds and glucosamine-6-phosphate synthase using molecular docking. The binding affinities of ligand **1** and ligand **2** molecules were determined as -7.1 and -7.3 kcal/mol, respectively. This study could be extended using derivatives of ligand having different substituent on benzene ring to find different candidates in drug development.

Authors' Contributions

All authors contributed equally to the study.

Statement of Conflicts of Interest

There is no conflict of interest between the authors.

Statement of Research and Publication Ethics

The author declares that this study complies with Research and Publication Ethics.

References

Ali, I., Burki, S., El-Haj, B. M., Shafiullah, Parveen, S., Nadeem, H. Ş., Nadeem, S., & Shah, M. R. (2020). Synthesis and characterization of pyridine-based organic salts: Their antibacterial, antibiofilm and wound healing activities. *Bioorganic Chemistry*, *100*, 103937. doi: 10.1016/j.bioorg.2020.103937

Ali, M. T., Blicharska, N., Shilpi, J. A., & Seidel, V. (2018). Investigation of the anti-TB potential of selected propolis constituents using a molecular docking approach. *Scientific Reports*, *8:12238*, 1–8. doi: 10.1038/s41598-018-30209-y

Almutairi, M. S., Zakaria, A. S., Ignasius, P. P., Al-Wabli, R. I., Joe, I. H., & Attia, M. I. (2018). Synthesis, spectroscopic investigations, DFT studies, molecular docking and antimicrobial potential of certain new indole-isatin molecular hybrids: Experimental and theoretical approaches. *Journal of Molecular Structure*, *1153*, 333–345. doi: 10.1016/j.molstruc.2017.10.025

Askri, S., Dbeibia, A., McHiri, C., Boudriga, S., Knorr, M., Roulland, E., Laprévote, O., Saffon-merceron, N., & Gharbi, R. (2022). Antimicrobial activity and in silico molecular docking studies of pentacyclic spiro[oxindole-2,3′-pyrrolidines] tethered with succinimide scaffolds. *Applied Sciences*, *12*(1), 360. doi: 10.3390/app12010360

Backes, G. L., Jursic, B. S., & Neumann, D. M. (2015). Potent antimicrobial agents against azole-resistant fungi based on pyridinohydrazide and hydrazomethylpyridine structural motifs. *Bioorganic and Medicinal Chemistry*, *23*(13), 3397–3407. doi: 10.1016/j.bmc.2015.04.040

Banerjee, K., Gupta, U., Gupta, S., Wadhwa, G., Gabrani, R., Sharma, S. K., & Jain, C. K. (2011). Molecular docking of glucosamine-6-phosphate synthase in Rhizopus oryzae. *Bioinformation*, *7*(6), 285–290. doi: 10.6026/007/97320630007285

Becke, A. D. (1993). Density-functional thermochemistry. III. The role of exact exchange. *The Journal of Chemical Physics*, *98*(7), 5648–5652. doi: 10.1063/1.464913

Bedia, K. K., Elçin, O., Seda, U., Fatma, K., Nathaly, S., Sevim, R., & Dimoglo, A. (2006). Synthesis and characterization of novel hydrazide-hydrazones and the study of their structure-antituberculosis activity. *European Journal of Medicinal Chemistry*, *41*(11), 1253–1261. doi: 10.1016/j.ejmech.2006.06.009

BIOVIA, Dassault Systemes, Discovery Studio Modeling Environment, Release 2017, San Diego, Dassault Systemes ___ (2016).

Cai, Y., Wang, Z., Li, Z., Zhang, M., & Wu, J. (2011). (E)-1-(4-Methoxyphenyl)-3-(2,4,6-trimethoxyphenyl)prop-2-en-1-one. *Acta Crystallographica Section*, *E67*, o1432. doi: 10.1107/S1600536811017788

Cancès, E., Mennucci, B., & Tomasi, J. (1997). A new integral equation formalism for the polarizable continuum model: Theoretical background and applications to Isotropic and anisotropic dielectrics. *Journal of Chemical Physics*, *107*(8), 3032–3041. doi: 10.1063/1.474659

Chmara, H., & Borowski, E. (1986). Bacteriolytic effect of cessation of glucosamine supply, induced by specific inhibition of glucosamine-6-phosphate synthetase. *Acta Microbiologica Polonica*, *35*(1–2), 15–27.

David, K., Munoz-Muriedas, J., Sime, M., Steadman, J. G. A., Thewlis, R. E. A., Trani, G., & Walter, D. S. (2010). 5,6,7,8-TetrahvdroM.2,41triazolor4,3-alpvrazine derivatives as P2X7 modulators. *WO 2010/125102 Al*.

Demurtas, M., Baldisserotto, A., Lampronti, I., Moi, D., Balboni, G., Pacifico, S., Vertuani, S., Manfredini,

S., & Onnis, V. (2019). Indole derivatives as multifunctional drugs: Synthesis and evaluation of antioxidant, photoprotective and antiproliferative activity of indole hydrazones. *Bioorganic Chemistry*, *85*, 568–576. doi: 10.1016/j.bioorg.2019.02.007

Dennington, R., Keith, T., & Millam, J. (2009). GaussView, Version 5. Semichem Inc., Shawnee Mission. *Shawnee Mission KS, Semichem Inc.*

Ditchfield, R. (1974). Self-consistent perturbation theory of diamagnetism. *Molecular Physics: An International Journal at the Interface Between Chemistry and Physics*, *27*(4), 789–807. doi: 10.1080/00268977400100711

El Sayed, M. T., El-Sharief, M. A. M. S., Zarie, E. S., Morsy, N. M., Elsheakh, A. R., Nayel, M., Voronkov, A., Berishvili, V., Sabry, N. M., Hassan, G. S., & Abdel-Aziz, H. A. (2018). Design, synthesis, anti-inflammatory antitumor activities, molecular modeling and molecular dynamics simulations of potential naprosyn® analogs as COX-1 and/or COX-2 inhibitors. *Bioorganic Chemistry*, *76*, 188–201. doi: 10.1016/j.bioorg.2017.11.002

Fikrika, H., Ambarsari, L., & Sumaryada, T. (2016). Molecular Docking Studies of Catechin and Its Derivatives as Anti-bacterial Inhibitor for Glucosamine-6-Phosphate Synthase. *IOP Conference Series: Earth and Environmental Science*, *31*(1), 012009. doi: 10.1088/1755-1315/31/1/012009

Filimonov, D. A., Lagunin, A. A., Gloriozova, T. A., Rudik, A. V., Druzhilovskii, D. S., Pogodin, P. V., & Poroikov, V. V. (2014). Prediction of the biological activity spectra of organic compounds using the pass online web resource. *Chemistry of Heterocyclic Compounds*, *50*(3), 444–457. doi: 10.1007/s10593-014-1496-1

Frisch, M. J., Trucks, G. W., Schlegel, H. B., & G. E. Scuseria, et al. (2009). Gaussian 09, Revision C.01. *Gaussian Inc. Wallingford, CT*.

Fun, H. K., Chantrapromma, S., & Suwunwong, T. (2011). (2E)-1-(Pyridin-2-yl)-3-(2,4,6-trimethoxyphenyl)prop-2-en-1-one. *Acta Crystallographica Section*, *E67*, o2789. doi: 10.1107/S1600536811039110

He, W. W., Yang, J., Ma, J. F., & Song, S. Y. (2012). Metal-dependent assemblies of an unusual pentanuclear cadmium cluster and a fascinating 3D 4-connected lead-containing framework. *Inorganic Chemistry Communications*, *24*, 63–66. doi: 10.1016/j.inoche.2012.07.044

Kandasamy, M., Mak, K.-K., Devadoss, T., Thanikachalam, P. V., Sakirolla, R., Choudhury, H., & Pichika, M. R. (2019). Construction of a novel quinoxaline as a new class of Nrf2 activator. *BMC Chemistry*, *13*(1), 1–10. doi: 10.1186/s13065-019-0633-4

Khalil, N. A., Ahmed, E. M., Mohamed, K. O., & Zaitone, S. A. B. (2013). Synthesis of new nicotinic acid derivatives and their evaluation as analgesic and anti-inflammatory agents. *Chemical and Pharmaceutical Bulletin*, *61*(9), 933–940. doi: 10.1248/cpb.c13-00261

Kotb, E. R., Soliman, H. A., Morsy, E. M. H., & Abdelwahed, N. A. M. (2017). New pyridine and triazolopyridine derivatives: Synthesis, antimicrobial and antioxidant evaluation. *Acta Poloniae Pharmaceutica - Drug Research*, *74*(3), 861–872.

Lee, C., Yang, W., & Parr, R. G. (1988). Development of the Colle-Salvetti correlation-energy formula into a functional of the electron density. *Physical Review B*, *37*, 785–789.

More, U. A., Joshi, S. D., Aminabhavi, T. M., Gadad, A. K., Nadagouda, M. N., & Kulkarni, V. H. (2014). Design, synthesis, molecular docking and 3D-QSAR studies of potent inhibitors of enoyl-acyl carrier protein reductase as potential antimycobacterial agents. *European Journal of Medicinal Chemistry*, *71*, 199–218. doi: 10.1016/j.ejmech.2013.11.004

Morjan, R. Y., Mkadmh, A. M., Beadham, I., Elmanama, A. A., Mattar, M. R., Raftery, J., Pritchard, R. G., Awadallah, A. M., & Gardiner, J. M. (2014). Antibacterial activities of novel nicotinic acid hydrazides and their conversion into N-acetyl-1,3,4-oxadiazoles. *Bioorganic & Medicinal Chemistry Letters*, *24*, 5796–5800. doi: 10.1016/j.bmcl.2014.10.029

Morris, G. M., Huey, R., Lindstrom, W., Sanner, M. F., Belew, R. K., Goodsell, D. S., & Olson, A. J. (2009). AutoDock4 and AutoDockTools4: Automated Docking with Selective Receptor Flexibility. *Journal of Computational Chemistry*, *30*(16), 2785–2791. doi: 10.1002/jcc.21256

Mouilleron, S., Badet-Denisot, M. A., & Golinelli-Pimpaneau, B. (2008). Ordering of C-terminal Loop and Glutaminase Domains of Glucosamine-6-Phosphate Synthase Promotes Sugar Ring Opening and Formation of the Ammonia Channel. *Journal of Molecular Biology*, *377*(4), 1174–1185. doi: 10.1016/j.jmb.2008.01.077

Muluk, M. B., Dhumal, S. T., Rehman, N. N. M. A., Dixit, P. P., Kharat, K. R., & Haval, K. P. (2019). Synthesis, Anticancer and Antimicrobial Evaluation of New (E)-N′-Benzylidene-2-(2-ethylpyridin-4-yl)-4-methylthiazole-5-carbohydrazides. *ChemistrySelect*, *4*(31), 8993–8997. doi:

10.1002/slct.201902030

Narang, R., Narasimhan, B., Sharma, S., Sriram, D., Yogeeswari, P., Clercq, E. De, Pannecouque, C., & Balzarini, J. (2011). Nicotinic Acid Benzylidene/Phenyl-Ethylidene Hydrazides: Synthesis, Antimicrobial Evaluation and QSAR Studies. *Letters in Drug Design & Discovery*, *8*(8), 733–749. doi: 10.2174/157018011796575999

Narang, R., Narasimhan, B., Sharma, S., Sriram, D., Yogeeswari, P., De Clercq, E., Pannecouque, C., & Balzarini, J. (2012). Synthesis, antimycobacterial, antiviral, antimicrobial activities, and QSAR studies of nicotinic acid benzylidene hydrazide derivatives. *Medicinal Chemistry Research*, *21*(8), 1557–1576. doi: 10.1007/s00044-011-9664-7

Neuman, D. M. (2018). *Antimicrobial pyridinohydrazide and hydrazomethylpyridine-based agents* (US 2018/0072672 A1).

Pomarnacka, E., Bednarski, P. J., Reszka, P., Dziemidowicz-Borys, E., Bieńczak, A., Werel, W., & Hałasa, R. (2006). Synthesis and biological activity of new 2-amino-8-chloro-5,5-dioxo[1,2,4]triazolo[2,3-b][1,4,2]benzodithiazines. *European Journal of Medicinal Chemistry*, *41*(5), 633–639. doi: 10.1016/j.ejmech.2005.11.009

Ragavendran, J. V., Sriram, D., Patel, S. K., Reddy, I. V., Bharathwajan, N., Stables, J., & Yogeeswari, P. (2007). Design and synthesis of anticonvulsants from a combined phthalimide-GABA-anilide and hydrazone pharmacophore. *European Journal of Medicinal Chemistry*, *42*(2), 146–151. doi: 10.1016/j.ejmech.2006.08.010

Shah, N., & Soman, S. (2018). Design , synthesis and evaluation of antimicrobial and anticancer activity of novel 3-aminomethyl pyridin derivatives. *European Journal of Pharmaceutical and Medical Research*, *5*(10), 229–241.

Shyma, P. C., Kalluraya, B., Peethambar, S. K., Telkar, S., & Arulmoli, T. (2013). Synthesis, characterization and molecular docking studies of some new 1,3,4-oxadiazolines bearing 6-methylpyridine moiety for antimicrobial property. *European Journal of Medicinal Chemistry*, *68*, 394–404. doi: 10.1016/j.ejmech.2013.07.019

Soujanya, M., & Rajitha, G. (2017). CODEN (USA): PCHHAX Synthesis , Characterization , Molecular Docking and Antimicrobial Activity of Nicotinic Acid Derived N-acylhydrazones. *Der Pharma Chemica*, *9*(17), 10–15.

Tok, F., Uğraş, Z., Sağlık, B. N., Özkay, Y., Kaplancıklı, Z. A., & Koçyiğit-Kaymakçıoğlu, B. (2021). Novel 2,5-disubstituted-1,3,4-oxadiazole derivatives as MAO-B inhibitors: Synthesis, biological evaluation and molecular modeling studies. *Bioorganic Chemistry*, *112*, 104917. doi: 10.1016/j.bioorg.2021.104917

Trott, O., & Olson, A. J. (2010). AutoDock Vina: Improving the Speed and Accuracy of Docking with a New Scoring Function, Efficient Optimization, and Multithreading. *Journal of Computational Chemistry*, *31*, 455–461. doi: 10.1002/jcc.21334

Ukrainets, I. V., Sidorenko, L. V., & Golovchenko, O. S. (2007). 4-Hydroxy-2-quinolones 132. Synthesis, chemical, and biological properties of 1-R-4-hydroxy-2-oxo-1,2-dihydroquinoline-3-carboxylic acids 2-nitrobenzylidenehydrazides. *Chemistry of Heterocyclic Compounds*, *43*(11), 1434–1439. doi: 10.1007/s10593-007-0221-8

Wang, S., Liu, H. Y., Xu, R. F., & Sun, J. (2017). Synthesis, biological evaluation, and molecular docking studies of diacylhydrazine derivatives possessing 1,4-benzodioxan moiety as potential anticancer agents. *Russian Journal of General Chemistry*, *87*(11), 2671–2677. doi: 10.1134/S1070363217110238

Wolinski, K., Hinton, J. F., & Pulay, P. (1990). Efficient Implementation of the Gauge-Independent Atomic Orbital Method for NMR Chemical Shift Calculations. *Journal of the American Chemical Society*, *112*(23), 8251–8260. doi: 10.1021/ja00179a005

World Health Organization WHO. (2021). Retrieved from https://www.who.int/news-room/fact-sheets/detail/antimicrobial-resistance

Wu, J., Zhang, L., Wang, J., Yang, S., & Li, X. (2009). 1-Phenyl-3-(2,4,6-trimethoxy-phen-yl)prop-2-en-1-one. *Acta Crystallographica Section*, *E65*, o2805. doi: 10.1107/S1600536809041877